Measurement of the Adiabatic Index in Be Compressed by Counterpropagating Shocks

C. Fortmann,[1,2] H. J. Lee,[3] T. Döppner,[1] R. W. Falcone,[4] A. L. Kritcher,[1] O. L. Landen,[1] and S. H. Glenzer[1]

[1]*Lawrence Livermore National Laboratory, Livermore, California 94551, USA*
[2]*Department of Physics and Astronomy, University of California, Los Angeles, California 90095, USA*
[3]*SLAC National Accelerator Laboratory, 2575 Sand Hill Road, Menlo Park, California 94025, USA*
[4]*Department of Physics, University of California, Berkeley, California 94720, USA*

(Received 1 July 2011; published 25 April 2012)

We report on the first direct measurement of the adiabatic index γ through x-ray Thomson scattering from shock-compressed beryllium. 9 keV x-ray photons probe the bulk properties of matter during the collision of two counterpropagating shocks. This novel experimental technique determines γ by using only the measured mass densities and vanishing particle velocity at the point of shock collision to close the Rankine-Hugoniot equations. We find $\gamma > 5/3$ at $3\times$ compression, clearly different from ideal gas behavior. At $6\times$ compression, γ shows the convergence to the ideal gas limit, in agreement with linear scaling laws.

DOI: 10.1103/PhysRevLett.108.175006 PACS numbers: 52.25.Os, 52.70.La, 64.30.−t, 65.40.Ba

Compression of solid targets by intense laser radiation generates superdense matter with many times solid density, temperatures of several 10 000 K, and pressures in excess of 1 Mbar. These extreme states of matter serve as model systems to investigate astrophysical objects that exist at similar conditions. Studying the equation of state (EOS) of matter at extreme conditions is vital for inertial confinement fusion [1] experiments, where matter is compressed up to 1000 g/cm^3. The adiabatic index, i.e., the shock $\gamma = 1 + p/\rho\varepsilon$, with pressure p, mass density ρ, and energy density ε [2], is a central quantity. For perfect gases, γ is the ratio of heat capacities at constant pressure and volume c_p/c_v, respectively, and can also be expressed through the sound speed $\gamma = \gamma_S = c_s^2\rho/p$. In nonideal dense plasmas, the shock γ, sound speed γ, and the heat capacities become density-dependent and are no longer equal.

Beryllium is a candidate capsule ablator material in inertial confinement fusion experiments [3]. Knowledge of its thermodynamical properties and transport properties (thermal and electric conductivity) at extreme density, pressure, and temperature are thus of high interest.

Spectrally resolved x-ray Thomson scattering (XRTS) [4] provides accurate measurements of electron density and temperature in isochorically heated [5] and compressed matter via the shape of the plasmon resonance [6,7] and the Compton feature [8]. In the Compton scattering regime, at a large scattering angle, the plasma response is essentially uncorrelated, and the Compton profile reflects the single-particle distribution function which is fully characterized by electron density n_e and temperature T. Inferring these parameters by fitting the Compton profile calculated from first principles is, hence, model-independent. Moreover, the electron temperature is constrained by the amount of elastic (Rayleigh) scattering. Finally, the average ionization per ion and, hence, the mass density are measured by observing Compton scattering from bound electrons visible at large energy shifts, where free-free scattering is suppressed.

In this Letter, we present a novel method to directly infer information about the EOS of strongly compressed matter by using XRTS. A beryllium sample is symmetrically compressed by two counterpropagating shock waves of equal strength producing densities of 3 and 6 times the solid density before and after the shock collision, respectively. In this Fermi degenerate plasma, the width of the Compton scatter profile provides a measure of the electron density n_e and is only weakly sensitive to the temperature. Thus, measuring the first and second mass compression ratios, we obtain sufficient information to infer γ at both instants. We solve the Rankine-Hugoniot equations for colliding shocks that govern the pressure and density jump across the shock-front discontinuity and which contain γ as a parameter. Our results show that γ assumes relatively high values of $1.9(+0.7/-0.3)$ in the high compression regime, in agreement with a simple scaling model for γ [9] that is implemented, e.g., in the SESAME EOS tables [10]. Within the error bars, this high compression value is consistent with the ideal gas limit $\gamma = 5/3$.

The experiment has been carried out at the Omega Laser at Laboratory for Laser Energetics, University of Rochester. Beryllium foils of 250 μm thickness are symmetrically compressed by interaction with high energy laser pulses. A photograph of the target is shown in Fig. 1(a), and Fig. 1(b) shows the setup. The Be foil is radiated from both sides by a total of 12 laser beams operating at 351 nm wavelength (3ω). Each beam delivers up to 480 J in a 1 ns long flattop pulse onto a common focal spot of 800 μm in diameter. Use of continuous phase plates yields a homogenous intensity profile across the focal spot. The pulses are staggered in time, producing a constant intensity of 2.0×10^{14} W/cm^2 for 3 ns as shown in Fig. 1(c) together with the resulting mass density

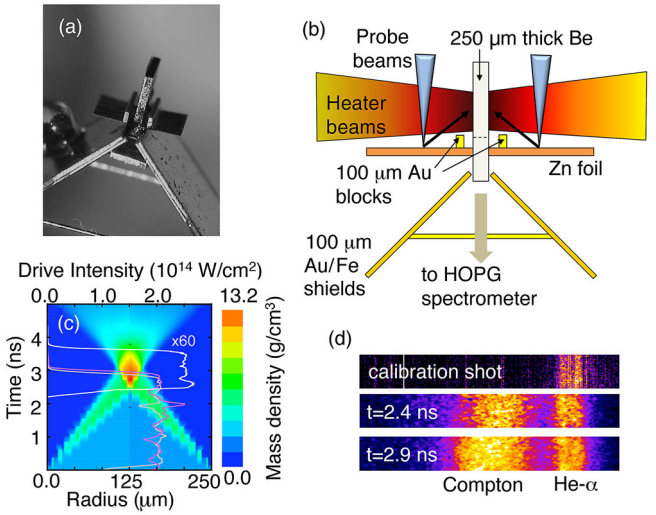

FIG. 1 (color online). (a) Photograph of the target. (b) Experimental setup. (c) Rad-hydro simulation of the mass density evolution. Drive beam intensity profiles for each side (gray and purple) and x-ray probe pulse (white) are overlaid. (d) Raw x-ray scattering data. Top to bottom: Calibration shot, measuring the Zn He-α doublet; scattering before and after shock collision showing elastic and Compton scattering; increased Compton width is observed after shock collision.

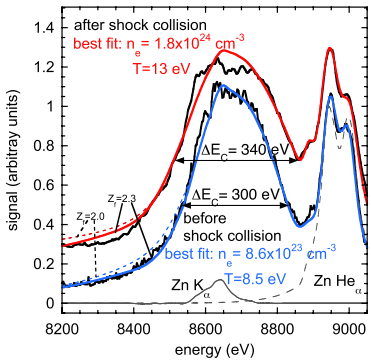

FIG. 2 (color online). XRTS spectra before ($t = 2.4$ ns) and after ($t = 2.9$ ns) shock collision (+ 0.2 offset). XRTS simulations for the best-fit values for electron density $n_e = 8.6 \times 10^{23}$ cm^{-3} and temperature $T = 9$ eV (blue) and $n_e = 1.8 \times 10^{24}$ cm^{-3}, $T = 13$ eV (red). $Z_f = 2.3$ in both calculations; thin dashed lines: $Z_f = 2.0$. Zn He-α spectrum (black dashed line) and the Zn $K\alpha$ line (solid gray line).

evolution as simulated by the 1D radiation-hydrodynamics code HELIOS [11], applying the PROPACEOS EOS model.

Simulations indicate that the shock waves collide in the target's center after 2.8 ns. Density and temperature conditions are homogeneous over spatial extensions of 25 μm in the horizontal direction.

The plasma conditions are probed with x-ray Compton scattering [4] by laser produced Zn He-α radiation (photon energies of $E_0 = 8.95$ and 8.99 keV for Zn He-α_1 and He-α_2, respectively) and 140° ± 10° scattering angle. In the single-compressed matter, electron density of $n_e = 8.6 \times 10^{23}$ cm^{-3} is observed, rising to 1.8×10^{24} cm^{-3} at shock collision. High energy lasers produce the Zn He-α radiation. Pulses of 480 J energy and 1.0 ns duration are focused onto a Zn foil (200 μm diameter focus), yielding intensities of $\approx 1.5 \times 10^{16}$ W/cm^2. The x-ray probe beams start 2.5 ns after the heater beams. At $\theta = 140° \pm 10°$ scattering angle, the resulting k vector is $k = 2E_0 \sin(\theta/2)/\hbar c = (8.4 \pm 0.2)$ Å^{-1}. In Fig. 2, we show x-ray scattering spectra from compressed targets at 2.4 and 2.9 ns after the drive beam-target interaction, i.e., before and after shock collision, respectively. These x-ray spectra are measured by dispersing the scattered radiation in a large graphite crystal (highly oriented pyrolytic graphite) onto an x-ray framing camera with 0.18 ns temporal resolution. A 100 μm thick gold shield blocks the direct view of the spectrometer crystal to the intense x-ray probe source.

We observe elastic Rayleigh scattering from Zn He-α radiation at 8.95 and 8.99 keV along with a smaller contribution from Zn $K\alpha$ radiation at 8640 eV. From the integrated Rayleigh feature, we determine the plasma temperature by using the high-k limit (Debye-Hueckel model) for the ion-ion structure factor and the screening cloud [12]. We find $T = (10 \pm 2)$ eV before shock collision and $T = (15 \pm 2)$ eV after shock collision. Results of this analysis are shown in the Supplemental Material [13].

Compton scattering from bound and free electrons is measured at a Compton shift of $E_C = \hbar^2 k^2/2m_e \simeq 270$ eV. The width of the Compton peak substantially increases upon shock collision from $\Delta E_C = 300$ eV to $\Delta E_C = 340$ eV. The Compton width depends on $\sqrt{E_F} \propto n_e^{1/3}$ in this partly Fermi degenerate regime, where $k_B T/E_F \simeq 0.3$, $E_F = \hbar^2(3\pi^2 n_e)^{2/3}/2m_e = 31$ eV(52 eV) is the electron Fermi energy before (after) shock collision.

By comparing our experimental scattering spectra to calculations for the dynamical structure factor [4], we infer n_e and T. The data indicate that we are in the noncollective (Compton scattering) regime with scattering parameter $\alpha = 1/k\lambda_s = 0.15$ (λ_s is the plasma screening length). In this regime, two-body correlations are negligible; the structure factor is only a function of n_e and T without any model dependence. Figure 3 shows contour lines for the

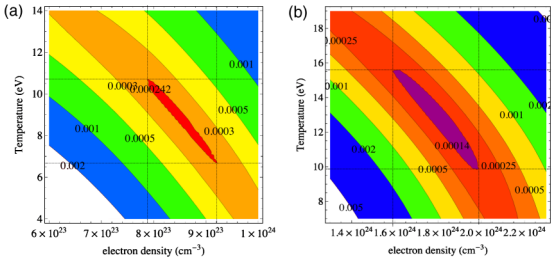

FIG. 3 (color online). Contour lines for the mean square variance between fit curves and scattering data as a function of n_e and T. The innermost contours define the error bars on n_e and T. (a) Before shock collision, (b) after shock collision.

mean square variance between fit curves and scattering data as a function of n_e and T. From this analysis we obtain $n_e = (8.6 \pm 0.7) \times 10^{23}$ cm^{-3} and $T = (9 \pm 2)$ eV before shock collision and $n_e = (1.8 \pm 0.2) \times 10^{24}$ cm^{-3} and $T = (12 \pm 3)$ eV after shock collision, consistent with the temperature measurements using the Rayleigh peak.

Compton scattering from K-shell electrons contributes at photon energies below 8890 eV, corresponding to the K-shell ionization potential of ~110 eV in the dense plasma, where continuum lowering of ~60 eV is taken into account via the Stewart-Pyatt model [14]. The amount of bound-free scattering depends on the average ionization. We obtain good agreement with the data assuming $Z_f = 2.3$, consistent with earlier XRTS measurements of isochorically heated and shock-compressed Be [5,15]. For single-shock conditions similar to ours, Lee *et al.* [8] report $Z_f = 2.0$. However, calculations for $Z_f = 2.0$ (thin dashed lines in Fig. 2) overpredict the bound-free contribution. Even at increased electron density during shock collision, ionization potential lowering is below 10 eV with respect to the single shocked state as estimated through the Stewart-Pyatt model. Hence, changes in Z_f between single and double shocked states are expected to be below the experimental resolution.

Correspondingly, the mass density rises from $\rho_1 = (5.6 \pm 0.7)$ g/cm^3 to $\rho_2 = (11.7 \pm 1.9)$ g/cm^3. The uncertainties in ρ are the sum of uncertainties resulting from the n_e fitting procedure (see Fig. 3) and 5% uncertainty in Z_f. The compression increases from $\rho_1/\rho_0 = 3.0$ to $\rho_2/\rho_0 = 6.3$, with respect to the solid mass density $\rho_0 = 1.85$ g/cm^3. Here and in the following, we denote conditions in the uncompressed material by the index 0, the single shock-compressed matter by index 1, and the region of shock overlap by index 2.

We apply the Rankine-Hugoniot equations [16] to determine the adiabatic index γ. The Rankine-Hugoniot equations follow from the conservation of total mass, energy, and momentum. They relate the particle velocities u_0 and u_1, pressures p_0 and p_1, and mass densities p_0 and p_1 in the uncompressed and in the compressed region, respectively. One finds for the energy jump across the shock front

$$\varepsilon_0 - \varepsilon_1 = (p_0 + p_1)(1/\rho_1 - 1/\rho_0)/2. \tag{1}$$

These relations hold for each individual shock as well as for the two shock fronts that evolve after the shock collision between the single and the doubly shocked material and which travel in opposite directions away from each other. The adiabatic index γ is introduced to eliminate the internal energy $\varepsilon = p/(\gamma - 1)\rho$. Accounting for different values of γ before and after compression, one derives for the compression ratio

$$\frac{\rho_1}{\rho_0} = \left[1 + \frac{p_1}{p_0}\frac{\gamma_1 + 1}{\gamma_1 - 1}\right] \Big/ \left[\frac{p_1}{p_0} + \frac{\gamma_0 + 1}{\gamma_0 - 1}\right]. \tag{2}$$

Preheat due to fast electrons generated on the target's surface is negligible: At our drive laser intensities, hot electrons with $\langle E_{\mathrm{hot}}\rangle = 3$ keV average energy, estimated by resonance absorption [17], penetrate only the first 9 μm [18]. Correspondingly, $p_0 \ll p_1$, we are in the strong shock limit, where one recovers the familiar result

$$\lim_{p_1/p_0 \to \infty} \frac{\rho_1}{\rho_0} = \frac{\gamma_1 + 1}{\gamma_1 - 1}. \tag{3}$$

Note that the strong shock compression depends only on γ_1, i.e., the conditions in the compressed region. For a perfect monatomic gas with $\gamma = 5/3$, one obtains $\lim_{p_1/p_0 \to \infty} \rho_1/\rho_0 = 4$. The residual level of density fluctuations due to shock induced turbulence after the first shock is estimated following Ref. [19] as $\sqrt{\langle \delta\rho\, \delta\rho \rangle}/\rho_1 \simeq 1\%$, i.e., within the experimental error bars. Undercompression due to turbulence is therefore neglected.

The jump in particle velocities can be expressed as

$$(u_i - u_j)^2 = (1 - \rho_i/\rho_j)(p_j/p_i - 1)p_i/\rho_i. \tag{4}$$

In the case of two colliding strong shocks, symmetry of the problem with respect to the contact surface between the two shock waves at the moment of collision completely determines the final compression [20]. In particular, the material at the contact surface is at rest, $u_2 = 0$. Furthermore, the material velocity in the unshocked material u_0 is negligible compared to u_1, the velocity in the first, strongly shocked material region. From the two forms of Eq. (4) corresponding to $|u_2 - u_1| = u_1$ and $u_1 = |u_1 - u_0|$, we find a quadratic equation for the compression ratio ρ_2/ρ_1:

$$\frac{2\frac{\rho_2}{\rho_1}\gamma_1\frac{\gamma_2 - 1}{\gamma_1 - 1} - 2\gamma_2}{\frac{\rho_2}{\rho_1}(1 - \gamma_2) + \gamma_2 + 1}\,\frac{\frac{\rho_2}{\rho_1} - 1}{\frac{\rho_2}{\rho_1}} = \frac{\rho_1}{\rho_0} - 1. \tag{5}$$

For a system with constant adiabatic index $\gamma_2 = \gamma_1 = \gamma_0$, one recovers the result $\frac{\rho_2}{\rho_1} = [2 + (\gamma + 1)(\frac{\rho_1}{\rho_0} - 1)]/[2 + (\gamma - 1)(\frac{\rho_1}{\rho_0} - 1)]$ for the second compression [20]. For the ideal gas $\frac{\rho_2}{\rho_1} = 2.5$.

Using our measured mass density values, we find the adiabatic indices γ_1 and γ_2 by inverting relations (3) and (5):

$$\gamma_1 = (\rho_1 + \rho_0)/(\rho_1 - \rho_0), \qquad \gamma_2 = \rho_2/(\rho_2 - \rho_1). \tag{6}$$

For the single-compressed Be before shock collision, we obtain $\gamma_1 = 2.0 \pm 0.2$ at $\rho_1 = (5.6 \pm 0.7)$ g/cm^3 and $\gamma_2 = 1.9^{+0.7}_{-0.4}$ at $\rho_2 = (11.7 \pm 1.9)$ g/cm^3 for the material after the collision.

Figure 4 shows our data (red points) for the adiabatic index reaching high densities of ~12 g/cm^3. Vertical error bars on γ_2 result from the dependence on ρ_1 and ρ_2. The black diamond-shaped point is inferred from the

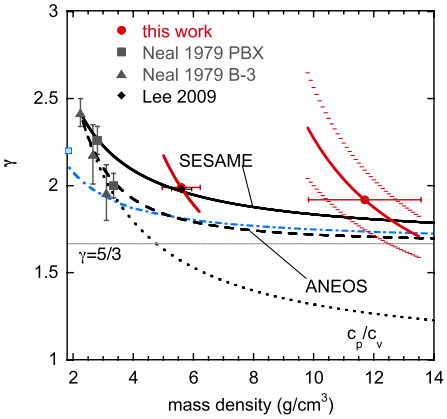

FIG. 4 (color online). Adiabatic index γ for compressed Be measured by XRTS (red points). Vertical error bars on the high compression point result from the dependence of γ_2 on ρ_1 and ρ_2. Black diamond: Compression data by Lee *et al.* Squares and triangles at low compression measurements of γ_S by Neal *et al.* Analytical expressions for γ_S used in SESAME EOS (solid line) and in the ANEOS model (dashed line) and linear model for c_p/c_v (dotted line). Dash-dotted (blue) line: DFT EOS simulation for γ_S; blue square: solid Be quoted by Rudin *et al.*

single-shock compression data from Lee *et al.* [8] in excellent agreement with our measurement before shock collision.

For comparison, we also show measurements of the sound speed γ_S from explosion experiments (squares and triangles) inferred through shock-wave radiography by Neal [21]. The two data sets correspond to different explosives used to generate the shock wave. Shock pressures in the 30 GPa range are reported, where Be is in the bcc phase. The dashed blue curve is a density-functional theory (DFT) simulation for γ_S [22] in hcp Be; the blue square is the experimental point for γ_S for solid hcp Be as quoted by the same authors. The black solid curve is an analytic expression for γ_S that is implemented in the generator of the SESAME EOS tables [10], $\gamma_S(\rho) = \gamma_S(\rho_0)\rho_0/\rho + 5(1 - \rho_0/\rho)/3$ [9]; the black dashed curves are taken from the ANEOS model [23], which assumes quadratic scaling in ρ/ρ_0 instead of the linear behavior implemented in SESAME. The reference point (ρ_0, γ_0) is fixed at the point for lowest compression reported by Neal. These theoretical models converge to the high density (Fermi degenerate) limit $\gamma(\rho \gg \rho_0) = 1.67$. Also our data seem to go to that limit, although more slowly. Finally, the dotted (black) curve is a linear scaling model for the ratio of heat capacities $c_p/c_v = 1 + [(c_p/c_v)_0 - 1]\rho_0/\rho$; at high densities, $c_p/c_v = 1$ [24].

Our results clearly demonstrate that the adiabatic index is significantly different from the heat capacity ratio. The SESAME model for γ_S with respect to the lowest compression point by Neal lies within the error bars for both single and double shocked Be but tends to slightly underestimate γ. The ANEOS model and the DFT simulation for γ_S are not consistent with our shock-γ measurements at single compression. At high compression, all models converge to the ideal gas 5/3 and are consistent with our data within the error bars. On the other hand, data from Neal at increased compression agree only with the ANEOS model and also with the c_p/c_v scaling.

We found $\gamma = 1 + p/\rho\varepsilon$ being substantially higher than 5/3 at single compression, which means in turn that $p/\rho\varepsilon$ exceeds the ideal gas value 2/3. This is in agreement with quantum mechanical EOS calculations for dense, partly degenerate plasmas [25]. Exchange contributions are the dominant terms, leading to a decrease in pressure and in internal energy, the latter being much more pronounced (up to 80% with respect to the ideal gas value vs 10% reduction in pressure). The net effect is an increase in the adiabatic index $\gamma = 1 + p/\rho\varepsilon$. Also at double compression, the relatively high value for $\gamma_2 = 1.9$ would indicate a reduced single-shock compressibility [cf. Eq. (3)] by 20% with respect to $\gamma = 5/3$. However, $\gamma = 5/3$ is still consistent with our data within the error bars, and a decisive statement cannot be made.

In conclusion, we have measured the mass density increase in Be upon shock compression by two counterpropagating shock waves before and after the shock collision. From the Hugoniot relations, we inferred γ at two mass densities. Our results agree with a linear model used in the SESAME EOS. They show the departure from the ideal gas behavior $\gamma = c_p/c_v$ at single-shock compression, consistent with a reduction in internal energy due to the exchange interaction in partly degenerate plasmas. The presented novel technique has great potential for applications in material research, inertial confinement fusion, and laboratory astrophysics. To this end, we need to improve the resolution in the mass density measurement by reducing the Zn $K\alpha$ emission and by taking an average over multiple shots to increase the signal to noise ratio. We also plan to perform high-precision measurements using x-ray free electron laser radiation where we take advantage of the larger photon number at smaller bandwidth to improve signal to noise and increase the separation between inelastic and elastic scattering components, allowing for a more detailed and accurate density and temperature measurement.

This work was performed under the auspices of the U.S. Department of Energy by Lawrence Livermore National Laboratory under Contract No. DE-AC52-07NA27344 and supported by LDRD Grant No. 10-ER-050. C. F. acknowledges support by the Alexander von Humboldt Foundation. We thank A. Pak and L. Divol for helpful discussions.

[1] J. D. Lindl, P. Amendt, R. L. Berger, S. G. Glendinning, S. H. Glenzer, S. W. Haan, R. L. Kauffman, O. L. Landen, and L. J. Suter, Phys. Plasmas **11**, 339 (2004).
[2] R. P. Drake, *High Energy Density Physics* (Springer, New York, 2006).

[3] D. C. Wilson, Phys. Plasmas **5**, 1953 (1998).
[4] S. H. Glenzer and R. Redmer, Rev. Mod. Phys. **81**, 1625 (2009).
[5] S. H. Glenzer, O. L. Landen, P. Neumayer, R. W. Lee, K. Widmann, S. W. Pollaine, R. J. Wallace, G. Gregori, A. Höll, T. Bornath, R. Thiele, V. Schwarz, W.-D. Kraeft, and R. Redmer, Phys. Rev. Lett. **98**, 065002 (2007).
[6] A. L. Kritcher, P. Neumayer, J. Castor, T. Döppner, R. W. Falcone, O. L. Landen, H. J. Lee, R. W. Lee, E. C. Morse, A. Ng, S. Pollaine, D. Price, and S. H. Glenzer, Science **322**, 69 (2008).
[7] P. Neumayer, C. Fortmann, T. Döppner, P. F. Davis, R. W. Falcone, A. L. Kritcher, O. L. Landen, H. J. Lee, R. W. Lee, C. Niemann, S. Le Pape, and S. H. Glenzer, Phys. Rev. Lett. **105**, 075003 (2010).
[8] H. J. Lee, P. Neumayer, J. Castor, T. Döppner, R. W. Falcone, C. Fortmann, B. A. Hammel, A. L. Kritcher, O. L. Landen, R. W. Lee, D. D. Meyerhofer, D. H. Munro, R. Redmer, S. P. Regan, S. Weber, and S. H. Glenzer, Phys. Rev. Lett. **102**, 115001 (2009).
[9] L. Davison, *Fundamentals of Shock Wave Propagation in Solids* (Springer, Heidelberg, 2008).
[10] S. Lyon and J. Johnson, Los Alamos National Laboratory, Database Technical Report No. LA-UR-92-3407, 1992 (unpublished).
[11] J. MacFarlane, I. Golovkin, and P. Woodruff, J. Quant. Spectrosc. Radiat. Transfer **99**, 381 (2006).
[12] D. Kremp, M. Schlanges, and W.-D. Kraeft, *Quantum Statistics of Nonideal Plasmas* (Springer, Heidelberg, 2005).
[13] See Supplemental Material at http://link.aps.org/supplemental/10.1103/PhysRevLett.108.175006 for determination of the plasma temperature T from the elastic scattering component.
[14] J. C. Stewart and K. D. Pyatt, Jr., Astrophys. J. **144**, 1203 (1966).
[15] A. Kritcher, T. Döppner, C. Fortmann, O. Landen, R. Wallace, and S. Glenzer, High Energy Density Phys. **7**, 271 (2011).
[16] Y. Zel'Dovich and Y. Raizer, in *Physics of Shock Waves and High-Temperature Hydrodynamic Phenomena*, edited by W. D. Hayes and R. F. Probstein (Dover, Mineola, NY, 2002).
[17] W. Kruer, in *Handbook of Plasma Physics*, edited by A. Rubenchik and S. Witkowski (Westview, Amsterdam, 2003), Vol. 3.
[18] S. Atzeni, Phys. Plasmas **6**, 3316 (1999).
[19] G. Hazak, A. L. Velikovich, J. H. Gardner, and J. P. Dahlburg, Phys. Plasmas **5**, 4357 (1998).
[20] H. Motz, *The Physics of Laser Fusion* (Academic, London, 1979).
[21] T. Neal, in *High-Pressure Science and Technology, AIRAP Conference Proceedings*, edited by K. D. Timmerhaus and M. S. Barber (Plenum, New York, 1979), Vols. 1 and 2.
[22] S. P. Rudin, M. D. Jones, and J. D. Johnson, in *Proceedings of the Joint 20th AIRAPT and 43rd EHPRG International Conference on High Pressure Science and Technology* (Forschungszentrum Karlsruhe, Germany, 2005), p. O058.
[23] S. Thompson and H. S. Lawson, Sandia National Laboratories Technical Report No. SC-RR-710714, 1972 (unpublished).
[24] G. P. Horedt, *Polytropes—Applications in Astrophysics and Related Fields* (Kluwer Academic, Dordrecht, 2004).
[25] J. Vorberger, M. Schlanges, and W. D. Kraeft, Phys. Rev. E **69**, 046407 (2004).